Suitability of short-period sensors for retrieving reliable H/V peaks for frequencies less than 1 Hz.

Authors:

A. Strollo[1,2], S. Parolai[1], K.-H. Jäckel[1,3], S. Marzorati[4], D. Bindi[4]

Affiliation:

[1]GeoForschungsZentrum Potsdam, Potsdam, Germany

[2]University of Potsdam, Potsdam, Germany

[3]GIPP Geophysical Instrumental Pool Potsdam

[4]Istituto Nazionale di Geofisica e Vulcanologia, Sezione di Milano

Corresponding author address:

GeoForschungsZentrum Potsdam

A. Strollo, Telegrafenberg, 14473 Potsdam, Germany

Tel: +49 331 288 1285

Fax: +49 331 288 1204

strollo@gfz-potsdam.de

Abstract

Using three different short-period electromagnetic sensors with resonant frequencies of 1 Hz (Mark L4C-3D), 2 Hz (Mark L-22D), and 4.5 Hz (I/O SM-6), coupled with three digital acquisition system, the PDAS Teledyne Geotech, the REFTEK 72A, and the Earth Data Logger PR6-24 (EDL), the effect of the seismic instruments on the horizontal-to-vertical spectral ratio (H/V) using seismic noise for frequencies less than 1 Hz has been evaluated. For all possible sensors - acquisition system pairs, the background seismic signal and instrumental self-noise power spectral densities have been calculated and compared. The results obtained when coupling the short-period sensors with different acquisition systems show that the performance of the considered instruments at frequencies < 1 Hz strongly depends upon the sensor-acquisition system combination and the gain used, with the best performance obtained for sensors with the lowest resonance frequency. For all acquisition systems, it was possible to retrieve correctly the H/V peak down to 0.1-0.2 Hz by using a high gain and a 1 Hz sensor. In contrast, biased H/V spectral ratios were retrieved when low-gain values were considered. Particular care is required when using 4.5 Hz sensors since they may not even allow the fundamental resonance frequency peak to be reproduced.

Introduction

It is well known that subsurface geology can strongly affect both the amplitude and lengthening of the earthquake-induced ground shaking recorded at the Earth surface. The assessment and consideration of local site amplification effects is mandatory for studies aiming at seismic hazard assessment, such as the calibration of ground motion prediction equations (GrMPEs) or the determination of ground-shaking scenarios computed for different levels of source and propagation complexity. Since local geology can vary significantly over

distances of only a few hundreds meters, the assessment of site response within large urban areas may require measurements at a large number of sites.

Moreover, the chance of recording seismic events in earthquake-prone urban areas can be small, either due to a low signal-to-noise ratio or to a low rate of seismicity. Therefore, techniques that allow information about site response to be obtained without using earthquake recordings and at a low cost have recently gained popularity. Among these, the Nakamura technique (Nakamura, 1989) allows the estimation of the fundamental resonance frequency of a site from the peak in the horizontal-to-vertical (H/V) spectral ratio of microtremor measurements. The requirement of performing low-cost and rapid measurements therefore affects the choice of the equipment employed. For example, short-period sensors are often preferred to broad-band ones because of their ease of installation, their robust nature and their relatively low-cost. Due to budget limitations, microzonation studies based on seismic noise measurements are also performed by using low-cost, but lower dynamic range, acquisition system.

It follows that when microtremor measurements are used to infer information about the site response, it is necessary to evaluate the contribution to the recorded seismic signal of both the ambient seismic vibrations, that is the signal that carries information about the source generating it and the medium trough which it propagates, and of the self-noise of the instruments. In fact, high instrumental noise can limit the exploitability of the seismic noise at frequencies lower than the sensor corner frequency, affecting the estimate of the fundamental resonance frequency of a site from the peak in the H/V.

Previous studies were performed either to examine the effect of short-period sensors on the detection of the seismic noise signals at frequencies lower than 1 Hz (e.g. Riedesel et al., 1990; Rodgers, 1992, Rodgers, 1994) or to test the performance of different kinds of seismic sensors by directly comparing the results obtained from the inferred H/V spectral ratio (Mucciarelli, 1998; Parolai et al., 2001). Recently, a comparison of results obtained from

different kinds of acquisition systems and sensors was carried out by Guillier et al. (2007), with an experimental design optimized for investigating the effects in the higher frequency range (> 1 Hz).

In this study, differently from the previous ones, the effect of the acquisition system and sensor on the H/V peak, when it is expected to occur at frequencies lower than 1 Hz, is evaluated by considering three different short-period electromagnetic sensors with resonant frequencies of 1, 2, and 4.5 Hz coupled with three different digital acquisition systems.

In this work, for each considered sensor and acquisition system couple, the Power Spectral Density (PSD) of the instrumental self-noise is first calculated and compared with the PSD of recordings from a broad-band station, which was installed in the area of Cologne at a site where the resonance frequency is expected to be at about 0.2 Hz (Parolai et al., 2004). Next, the broad-band seismic noise signal is combined with the self-noise and the H/V spectral ratios calculated and compared with those obtained by the original broad-band recordings. Finally, the results are discussed and suggestions for an optimized seismic noise acquisition for H/V spectral ratio calculations are provided. In the following, so as to avoid confusion when using different terms that are synonymous (ambient seismic vibration, seismic noise, microtremor, ambient noise), ambient seismic vibration will refer to the input in our system (digital acquisition system plus sensor). The output will be defined as the background seismic signal, which is the input combined with the instrumental self-noise. Moreover, two acronyms will be used: SPES instead of short-period electromagnetic sensor and DAS instead of digital acquisition system.

Self-noise model and its reliability

Similarly to Rodgers (1994), the acceleration power self-noise model for a SPES is described by:

$$P_{sn}(f) = \frac{E_n(f) + Q_n}{|H(f)|^2} + S_n \qquad (\mathrm{m/s^2})^2/\mathrm{Hz} \qquad (1)$$

where S_n indicates the suspension noise, E_n the total electronic noise, Q_n the quantization noise, and $|H(f)|$ is the modulus of the transfer function of the SPES. The signal loss due to the voltage splitting between the coil resistance r_c and the damping resistor r_d is included in $|H(f)|$ using the open circuit generator constant G_g obtained multiplying G_s in Table 1 for : $\left(\frac{r_d}{r_c + r_d}\right)$

The suspension noise term S_n is calculated by:

$$S_n = 16\pi \frac{kT\zeta f_0}{M} \qquad (\mathrm{m/s^2})^2/\mathrm{Hz} \qquad (2)$$

where k is the Boltzmann's constant, T is the sensor temperature in degrees Kelvin (fixed to 293), ζ is the damping ratio, f_0 is the resonant frequency of the spring-mass system and M is the sensor mass.

The generalized total electronic noise E_n for the DAS considered in this study is

$$E_n(f) = 2V_{00}\left(\frac{f_{cv}}{f} + 1\right) + I_{00}\left(\frac{f_{ci}}{f} + 1\right) r_p^{\,2} + 4kTr_p \qquad \mathrm{V^2/Hz} \qquad (3)$$

where f_{cv} and f_{ci} are the corner frequencies for the voltage and current noise PSD, respectively. The resistor r_p is the parallel combination of the damping resistor r_d and the coil resistance r_c (all in ohms), V_{00} and I_{00} are the high frequency levels of the operational amplifier (op-amp) voltage and current noise PSDs, respectively, while the factor of 2 is introduced because the instruments we consider, have 2 op-amp in the input stage. Therefore, the voltage noise term is doubled.

The power spectral density of the quantization noise Q_n can be defined as:

$$Qn = \frac{\Delta^2}{12}\frac{1}{f_N} \qquad \mathrm{V^2/Hz} \qquad (4)$$

where Δ is the quantization interval, also called the least significant bit voltage of the DAS, and f_N is the Nyquist frequency (Sleeman et al., 2006). This formula defines the quantization

noise for an ideal analogue-digital converter (ADC) with no over-sampling and no digital anti-alias filtering. When the DASs are using ADCs of a sigma-delta type, as in our case, quantization noise can be empirically calculated by:

$$Qn = \frac{U^2{}_{peak}}{2} 10^{-SNR} \frac{1}{f_C} \qquad \mathrm{V^2/Hz} \qquad (5)$$

where U_{peak} is the peak input voltage, *SNR* is the full scale signal-to-noise ratio (dynamic range) in dB and f_C is the upper corner frequency of the (digital) anti-aliasing filter, typically ~ 0.8 f_N (Wesson, 2004). The signal-to-noise ratio varies with sampling rate, while the peak input voltage is inversely proportion to the gain. Generally, these *SNR* values for a specific sampling rate and U_{peak} values for a certain gain are available from the manufacturers. The Q_n values adopted in this work are for a fixed sampling rate of 100 samples/sec and the extreme values to which the pre-amplifier gain of each recording system can be set.

Figure 1 shows the self-noise PSD and the contribution of each term mentioned above when a EDL PR6-24 is coupled with the three SPESs, as well as the area delimited by the New Low Noise Model (NLNM) and New High Noise Model (NHNM) of Peterson (1993) (hereinafter called the Peterson Model). All parameters have been fixed according to Table 1 (SPES parameters) and Table 2 (DAS parameters). In the case of a gain of 1, the quantization noise Q_n is generally the dominant term for frequencies higher than 0.07, while setting the gain to 10 the electronic noise E_n is dominating especially in the low frequency range. Similarly, we find Q_n provides the larger contribution to the self-noise at low gain, and E_n dominates for high gains, for the REFTEK 72A, which uses the same amplifier as the EDL (Figure E1a, electronic appendix), and for the PDAS Teledyne Geotech (Figure E1b, electronic appendix) which uses a different amplifier. Variability in the results also depends upon the SPES that is connected to the DAS, especially for high gain values.

Due to the strong dependence of the results on the gain used, in the following, the calculations are carried out considering gains of 1 and 10 for the EDL, 1 and 32 for the REFTEK 72A, and 1 and 100 for the PDAS Teledyne Geotech, each representing extreme cases.

In order to validate the self-noise model proposed in this paper, one can obtain a measure of the self-noise by substituting the SPES with an ohmic resistor that has the same resistance as the coil. However, such a resistor will not exactly represent the electric impedance of the unlocked SPES, and therefore this procedure is not meant to precisely measure the electronic self-noise (Wielandt, 2002). Recently, Holcomb (1989) and Sleeman et al. (2006), proposed a method based on coherency analysis that requires the recording of background seismic signal using two identical instruments that operate side by side and are exposed to the same input. The main assumption of this method is that the coherent part of the recordings is the ambient seismic vibration, while the incoherent part is related to self-noise (same contribution for each SPES). The limits of the method are that a relatively quiet location (30-40 dB ambient seismic vibration / self-noise) as well as careful installation is required, since tilt or misalignment could produce additional incoherent noise. In order to verify the reliability of our theoretical estimates of self-noise PDS, that have the advantage of being easily and rapidly calculated for each possible DAS and SPES couple, the coherency test was carried out using two Mark L4-3C (1 Hz) connected to a 6-channel EDL PR6-24 (gain=10). The test was carried out in the Geodynamical Observatory Moxa (MOX) where the experimental conditions are optimal for this kind of test (http://www.geo.uni-jena.de/moxa). The obtained empirical self-noise curve is shown in Figure 2 and compared to that obtained from the theoretical approach. The excellent agreement of the results indicates the reliability of our theoretical estimates.

Data and H/V spectral ratio calculation

A network of 44 seismic stations was deployed in the Cologne area between the end of April and the beginning of June 2001, with the aim of recording local and regional seismicity, and ambient seismic vibration (Parolai et al., 2004). In this study, 30 minutes of ambient seismic vibration recorded on May 15th starting from midnight at the station K38, equipped with a Güralp CMG-3ESPD seismic acquisition system and broad-band sensor (all in one), are considered. Figure 3 (top panels) shows the selected ambient seismic vibration time series. The 30 minutes of recording are divided into windows of 81.92 seconds with no overlapping. For each window, linear trend in the data were removed and a 5% cosine tapering function was applied to both ends. The PSD of each window were then calculated following McNamara & Buland (2004) after applying a Fast Fourier Transform (FFT) to the data. In this study we consider only the vertical (UP) and north-south (NS) components of ground motion, although similar results can be obtained for the east-west component. Figure 3 (bottom panels) shows the UP and NS component PSDs calculated on the first window with the Peterson Model. Although night recordings were selected, their PSDs exceeds the NHNM in the frequency range between 1 and 3 Hz, which is the frequency range generally considered to be strongly affected by anthropogenic activity. This excess can be also related to the industrial activity in the neighbouring city of Cologne (Plesinger & Wielandt, 1974). The PSD in the frequency range between 0.1 and 1 Hz is characterized by microseismic activity (Gutenberg, 1921; for a recent review, see Webb 1998). The major areas for microseisms recorded in Germany had previously been identified as originating from the British and Norwegian costs (Gutenberg, 1921; Jung, 1934; more recently, Friedrich et al., 1998; Essen et al, 2003). The surface pressure map of the day of these recordings (e.g. http://www.wetterzentrale.de/topkarten/ fsreaeur.html) does not show any strong low pressure system over the North Sea. The absence of strong microseismic activity is also confirmed by values of PSD in the frequency range between 0.1 and 0.7 Hz which approach the NLNM. The behaviour of the lowest frequency part (below 0.1 Hz) of the horizontal component PSD

(down to 0.1 Hz) may be related to a tilt effect (Forbriger, 2006), due to the non optimal (temporary) installation of the broad-band sensor. However, a peak around 0.02 Hz is also mapped also in the time series (Figure 3 NS component) that may indicate the presence of infragravity waves (e.g. Webb, 1998).

In this work, the background seismic signal at the output of the DAS (output) is computed by summing, in the time domain, the selected ambient seismic vibration (input) window at station K38 with the SPES and DAS instrumental self-noise (self-noise), that we model using equations (1) to (5). The self-noise signal in the time domain is estimated from the self-noise PSD while considering a random distribution of the phase. That is, the input seismic summed to the self-noise in the time domain and the PSD of the expected output is calculated. The output was estimated in the time domain instead of simply summing the PSD of the input and self-noise, since for the short time windows generally used for H/V spectral ratio calculations, an effect due to the cross-term of the PSD of the resultant signal cannot be excluded, although by averaging a large number of spectra, this effect is expected to be averaged out (but such a large number of windows are not always available in H/V spectral ratio studies). A test we performed (not shown here) showed that the expected PSD noise computed either directly by summing the PSD of the input and self-noise, or by computing the PSD of their sum in the time domain, are almost the same, with the most pronounced differences for frequencies where the two PSDs cross. Since the tests we carried out showed that our conclusions about the influence of the chosen DAS and SPES on the H/V spectral ratio results will not depend upon the scheme adopted for computing the expected PSD noise, we preferred to adopt the scheme that better predicted what it is expected for the analysis of actual data. The PSD of the output is then computed for each combination of SPES and DAS. In all, 18 different combinations are considered (three SPESs, three DASs with two different gain values for each). Finally, the H/V was calculated for each PSD and then the logarithmic average of the

spectral ratios obtained after splitting the input windows into 20 non-overlapping segments, each having a duration of 81.92 s.

Results

The results of all 18 combinations are described in the following. However, for the sake of brevity, only those regarding the EDL and part of those for the REFTEK 72A are shown. The complete set of results is presented in the electronic appendix.

In general the results obtained for the different combinations of short-period SPES and DAS show that the performance of instruments at frequencies below 1 Hz strongly depends upon the combination of SPES, DAS and the gain used.

- *EDL PR6-24*

The PSD expected for a SPES connected to the EDL (Figure 4a) with the gain fixed to 1, shows the possibility of a Mark-L4-C-3D detecting input down to 0.1-0.2 Hz, as well as when the signal is approaching the NLNM. SPESs with a higher resonance frequency have less chance of correctly identifying input at lower frequencies (Figure 4b and 4c). In particular, using a 4.5 Hz SPES, the PSD of the input between 0.15 and 1 Hz can be retrieved from the output, only when the input level approaches the NHNM. For frequencies below 0.15 Hz, since the self-noise for the 4.5 Hz SPES is larger than the NHNM, the input characteristics cannot be retrieved using this type of SPES. The diminishing signal-to-noise ratio when increasing the resonance frequency of the SPES (Figure 4b and 4c) has a clear effect on the H/V spectral ratio. While the results obtained with a 1 Hz SPES (Figure 4a) agree well with those obtained by broad-band recordings, the H/V spectral ratio from 2 Hz-SPES recordings (Figure 4b) show an apparent shift of the resonant peak due to the intersection of the self-

noise PSD and the input PSD at about 0.2 Hz, also leading to lower S/N ratios at higher frequencies.

Both a large shift and a strong amplitude reduction of the H/V spectral ratio peak is shown when a 4.5 Hz SPES is used (Figure 4c). For the case of smaller spectral amplitudes (but still well within the NHNM and the NLNM), within this frequency range, the H/V spectral ratio of 4.5 Hz SPES would not show any peak at all. Finally, it is worth noting that below 0.1 Hz the H/V spectral ratio of the original broad-band recordings show a strong increase with decreasing frequency. This suggests a likely problem in the installation of the broad-band sensor, with this behaviour probably due to the tilt of the sensor (Forbriger, 2006).

Increasing the gain to 10 (Figure 4a, 4b and 4c) improves the ability to detect the spectral peaks in the ambient seismic vibration for the 4.5 Hz SPES, imitations in correctly retrieving the H/V spectral ratio peak are still observed for the 2 Hz and the 4.5 Hz SPESs.

- *REFTEK 72A*

The combination of the three SPESs with a REFTEK 72A (Figure E2a, E2b and E2c electronic appendix) while fixing the gain to 1 clearly shows a general worsening of the signal-to-noise ratio when compared to the same SPES and gain for the EDL case. In particular, a slight shift of the H/V spectral peak also affects the 1 Hz SPES results, while no peak at all is shown when a 4.5 Hz SPES is considered (Figure 5).

Increasing the gain to 32, allows us to obtain results similar to those derived using the EDL with the gain set to 10. This is due to the strong reduction of quantization noise due to the increase in the pre-amplifier gain (Equation (4) and Figure E1a electronic appendix).

- *PDAS Teledyne Geotech*

Results obtained considering the PDAS Teledyne Geotech (Figure E3a, E3b and E3c electronic appendix) and fixing the pre-amplifier gain to 1 are nearly identical to those obtained for REFTEK 72A when using gain 1. In this case, since the generalized total electronic noise E_n of the two DAS (although having different amplifiers with different f_{cv} , f_{ci},

V_{00} and I_{00}), as well as the quantisation noise Q_n, are very similar, nearly identical self-noise PSD are obtained.

When the gain is set to 100, the PDAS Teledyne Geotech provides results comparable with those obtained using an EDL and fixing the gain to 10, i.e. the best combination we found. The excellent performance of the PDAS Teledyne Geotech DAS is due to the strong reduction of the quantisation noise determined by increasing the gain (Figure E1b electronic appendix).

Conclusions

The main results from this study can be summarized as follow:

- 1 Hz SPESs can be used to detect ambient seismic vibration down to 0.2-0.1 Hz, but generally require a large gain. In fact, for the case where input is approaching the NLNM of Peterson (1993) and when the gain is fixed to 1, spectral amplitudes below 0.2 Hz can be masked by the self-noise.
- 1 Hz SPESs can be used for estimating the H/V spectral ratio down to at least 0.2 Hz, but in this case, using the maximum possible gain for the EDL, the REFTEK 72A, and the PDAS Teledyne Geotech, (10, 32, 100, respectively). When the minimum gain for the latter two DAS is used, a slight bias in the peak is observed. The successful use of these SPESs for estimating the H/V spectral ratio at lower frequencies (below 0.2 Hz) strongly depends upon the input amplitude.
- 2 Hz SPESs, combined with REFTEK 72A or PDAS Teledyne Geotech (setting the gain to 1), are not able to resolve ambient seismic vibration features at frequencies lower than 0.3 Hz for the case where the input is less than the average value between the NLNM and the NHNM of Peterson (1993).
- 2 Hz SPESs always provide biased H/V spectral ratios (shifting toward higher frequencies the peak) at frequencies lower than 0.3 Hz.

- 4.5 Hz SPESs cannot detect ambient seismic vibration for frequencies lower than 0.6 Hz if the gain is fixed to 1 (Figure 4c and E2c and E3c in electronic appendix). However, if a specially designed pre-amplifier is used, the performance of the 4.5 Hz sensor can be improved, increasing the S/N ratio to about 10 dB.
- The H/V spectral ratio peak at low frequencies obtained by the 4.5 Hz SPES recording is always biased and, for some combinations (e.g. REFTEK and PDAS), may even vanish.

The degree of bias in the H/V spectral ratio due to the DAS and SPES couple estimated in this study can be subject to variations, depending upon the level of input signal. However, the general tendency that was observed will still be valid. In particular, ambient seismic vibration recorded during periods of strong microseism might overstep the theoretical self-noise levels that we have calculated. However, we believe that our results provide a clear picture of the problems one can encounter when using certain seismic instruments. On the basis of these results, we suggest that when ambient seismic vibration in the frequency band between 0.1 and 1 Hz is of interest only, 1 Hz SPESs are preferred instead of 2 and 4.5 Hz SPESs. We also suggest that the ambient seismic vibration measured in the field should be compared with the instrumental self-noise PSD of the SPES-DAS combination, employed especially when high-resonance frequency SPESs are used.

In this paper, we tested 3 SPESs and 3 DASs, all of which are available on the market or still in use. Our results can be extended to SPESs and DASs with similar characteristics and, we hope, may encourage the investigation of the PSD of self-noise of other DASs that we have not considered.

Acknowledgements

K. Fleming kindly improved our English. We thank M. Picozzi for continuous stimulating discussions and comments on the manuscript. The comments of two anonymous reviewers and of the Associate Editor, J. Pujol, greatly improved the manuscript. Figures have been drawn using the GMT (Wessel & Smith, 1991) software. Identifying the name of the instruments' manufactures is not meant to be an endorsement of their products.

References

Essen, H.H., Krüger, F., Dahm, T. and Grevemeyer, I., 2003. On the generation of secondary microseisms observed in northern and central Europe, *Journal of geophysical Research*, 108, NO. B10, 2506, doi:10.1029/2002JB002338.

Forbriger, T., 2006. Low Frequency limit for H/V studies due to tilt, AG-Seismology session Oct. 04-06th 2006, Haidhof.

Friedrich, A., Krüger, F. and Klinge, K., 1998. Ocean generated microseismic noise located with the Gräfenberg array, *Journal of Seismology*, 47-64.

Guillier, B., Atakan, K., Chatelain, J.L., Havskov, J., Ohrnberger, M., Cara, F., Duval, A.M., Zacharopoulos, S., Teves-Costa, P. and The Sesame team, 2007. Influence of instruments on the H/V spectral ratio of ambient vibration, *Bulletin of Earthquake Engineering*, DOI 10.1007/s10518-007-9039-0.

Gutenberg, B., 1921. *Handbuch der Geophysik*, 4, 264:298.

Holcomb, L.G., 1989. A direct method for calculating instrument noise levels in side-by-side seismometer evaluations, *U.S. Geol. Surv, Open-File Rept,* 89-214.

http://www.geo.uni-jena.de/moxa

http://www.wetterzentrale.de/topkarten/ fsreaeur.html

Jung, K., 1934. Ueber mikrosesmische Unruhe und Brandung, *Zeitschr. F. Geophysik*, 10, 325-329.

McNamara, D.E. & Buland, R.P., 2004. Ambient noise levels in the continental United States, *Bull. Seismol. Soc. Am.,* 94(4), 1517-1527.

Mucciarelli, M., 1998. Reliability and applicability of Nakamura's technique using microtremors: an experimental approach, *Journal of Earth. Eng.* 2(4), 625-638.

Nakamura, Y., 1989. A method for dynamic characteristics estimations of subsurface using microtremors on the ground surface, *Q. Rept. RTRI Japan,* 30, 25-33.

Parolai, S., Bormann, P. and Milkereit, C., 2001. Assessment of the natural frequency of the sedimentary cover in the Cologne area (Germany) using noise measurements, *J. Earthquake Eng.,* 5(4), 541-564.

Parolai, S., Richwalski, S.M., Milkereit, C. and Bormann, P., 2004. Assessment of the stability of H/V spectral ratios and comparison with earthquake data in the Cologne area (Germany). *Tectonophysics,* 390, 57-73.

Peterson, J., 1993. Observations and modeling of seismic background noise, *U.S. Geol. Surv. Open-File Rept, 93-322*-95.

Plesinger, A. and Wielandt, E., 1974. Seismic noise at 2 Hz in Europe, *J. Geophys.,* 40, 131-136.

Riedesel, M.A., Moore, R. and Orcutt, J.A., 1990. Limits of sensitivity of inertial seismometers with velocity transducers and electronic amplifiers, *Bull. Seismol. Soc. Am*., 80(6), 1725-1752.

Rodgers, P.W., 1992. Frequency limits for seismometers as determined from signal-to-noise ratios. Part 1. The electromagnetic seismometer, *Bull. Seismol. Soc. Am*., 82(2), 1071-1098.

Rodgers, P.W., 1994. Self-noise spectra for 34 common electromagnetic seismometer/preamplifier pairs, *Bull. Seismol. Soc. Am.*, 84(1), 228-228.

Sleeman, R., Van Wettun, A. and Trampert, J., 2006. Three-channel correlation analysis: a new technique to measure instrumental noise of digitizers and seismic sensors, *Bull. Seismol. Soc. Am.,* 96(1), 258-271.

Wessel, P. and Smith, W.H.F., 1991. Free software helps map and display data *Eos. Trans. AGU* 72 (41), 441, 445-446.

Webb, S.C., 1998. Broadband seismology and noise under the ocean, *Reviews of Geophysics*, 36 (1), 105–142.

Wesson, V., 2004. http://www.seis.com.au/TechNotes/TN200410A_SNR.html, technical note.

Wielandt, E., 2002. Chapter 5: Seismic sensors and their calibration. In: Bormann, P. (Ed.) (2002). IASPEI New Manual of Seismological Observatory Practice, GeoForschungsZentrum Potsdam, Vol. 1, 46 pp.

Figure and table captions

Table 1: SPESs parameters.

Table 2: DASs parameters.

Figure 1: Comparing different components of self-noise for the EDL: Electronic Noise (E_n grey), Quantization Noise (Q_n black), Suspension Noise (S_n dashed black) and total self-noise (thick dashed grey); the grey shading indicates the area delimited by the NLNM and NHNM of Peterson (1993). Left: Results obtained for a gain equal to 1 and different SPESs. Right: Results obtained for a gain equal to 1o and different SPESs (1,2 and 4.5 Hz).

Figure 2: Comparison between estimates of theoretical self-noise (black) and experimental self-noise (grey) from the coherency test. The grey shading indicates the area delimited by the NLNM and NHNM of Peterson (1993).

Figure 3: (Top and middle) GURALP CMG-3ESPD broad-band recordings of ambient seismic vibration at the station K38 used in this study. (Bottom) PSD of the UP (black) and NS (grey) components of broad-band ambient seismic vibration recordings. Grey shading indicates the area delimited by NLNM and NHNM of Peterson (1993).

Figure 4a: Self-noise (dashed black), ambient seismic noise (input) from the broad-band recordings (black) and input plus self-noise PSD (thin grey) for the EDL DAS with gain=1 (left side) and gain=10 (right side) coupled with the 1 Hz SPES; the grey shading indicates the area delimited by the NLNM and NHNM of Peterson (1993). NS components are shown in the top panels while the UP components are in the centre. The bottom panels corresponding average H/V spectral ratio with 95% confidence interval of input from broad-band recordings (black) and average H/V spectral ratio with 95% confidence interval of input plus self-noise (grey).

Figure 4b: Same as Figure 5a but for the EDL coupled with a 2 Hz SPES.

Figure 4c: Same as Figure 5a but for the EDL coupled with a 4.5 Hz SPES.

Figure 5: H/V spectral ratio results for the REFTEK 72 A and different SPESs. Left: results for G=1. Right: results for G=32. Top: results for 1Hz SPESs. Bottom: results for 4.5 Hz SPESs.

Electronic Appendix captions

Figure E1a: Comparing different components of self-noise for the REFTEK 72A: Electronic Noise (E_n blue), Quantization Noise (Q_n light blue), Suspension Noise (S_n green) and total self-noise (thick dashed red); the grey shading indicates the area delimited by the NLNM and NHNM of Peterson (1993). Left: Results obtained for a gain equal to 1 and different SPESs. Right: Results obtained for a gain equal to 32 and different SPESs.

Figure E1b: Comparing different components of self-noise for the PDAS: Electronic Noise (E_n blue), Quantization Noise (Q_n light blue), Suspension Noise (S_n green) and total self-noise (thick dashed red); the grey shading indicates the area delimited by the NLNM and NHNM of Peterson (1993). Left: Results obtained for a gain equal to 1 and different SPESs. Right: Results obtained for a gain equal to 100 and different SPESs.

Figure E2a: Self-noise (red), ambient seismic noise (input) from broad-band recordings (blue) and input plus self-noise PSD (thin green) for the REFTEK 72A DAS with the gain=1 (left side) and the gain=32 (right side) coupled with a 1 Hz SPESs; the grey shading indicates the area delimited by the NLNM and NHNM of Peterson (1993). NS components are shown in the top panels while the UP components are in the centre. The bottom panels show the corresponding average H/V spectral ratio with 95% confidence interval of input from the broad-band recordings (blue) and average H/V spectral ratio with 95% confidence interval of input plus self-noise (green).

Figure E2b: Same as Figure 5a but for the REFTEK 72A coupled with a 2 Hz SPES.

Figure E2c: Same as Figure 5a but for the REFTEK 72A coupled with a 4.5 Hz SPES.

Figure E3a: Self-noise (red), ambient seismic noise (input) from broad-band recordings (blue) and input plus self-noise PSD (thin green) for PDAS DAS with the gain=1 (left side) and the gain 100 (right side) coupled with a 1 Hz SPES; the grey shading indicates the area delimited by the NLNM and NHNM of Peterson (1993). NS components are shown in the top panels while the UP components are in the centre. The bottom panels are the corresponding average H/V spectral ratio with 95% confidence interval of input from broad-band recordings (blue) and average H/V spectral ratio with 95% confidence interval of input plus self-noise (green).

Figure E3b: Same as Figure 5a but for the PDAS coupled with 2 Hz SPES.

Figure E3c: Same as Figure 5a but for the PDAS coupled with 4.5 Hz SPES

Short period electromagnetic sensor (SPES) Parameters

SPES	Freq. [Hz]	G_s [V/m/s]	ζ	M [Kg]	r_c [Ohms]	r_d [Ohms]	r_p [Ohms]
Mark L4C-3D	1,0	276,4	0,70	1,0000	5500,00	8900,00	3399,30
Mark L-22D	2,0	112,0	0,80	0,0728	5470,00	14300,00	3956,55
I/O SM-6	4,5	28,5	0,69	0,0111	375,00	10000,00	361,44

Table 1

Digital acquisition system (DAS) Parameters

DAS	Gain	Amplifier	V_{00} [V^2/Hz]	f_{cv} [Hz]	I_{00} [A^2/Hz]	f_{ci} [Hz]	Q_n [V^2/Hz]
EDL PR6-24	1	*OP-227*	9,00E-18	2,7	1,60E-25	140	7,22E-15
EDL PR6-24	10	*OP-227*	9,00E-18	2,7	1,60E-25	140	7,22E-17
REFTEK 72A	1	*OP-27*	9,00E-18	2,7	1,60E-25	140	3,02E-13
REFTEK 72A	32	*OP-27*	9,00E-18	2,7	1,60E-25	140	2,89E-16
PDAS	1	*OP-77*	1,00E-16	2,0	6,00E-26	200	2,50E-13
PDAS	100	*OP-77*	1,00E-16	2,0	6,00E-26	200	2,50E-17

Table 2

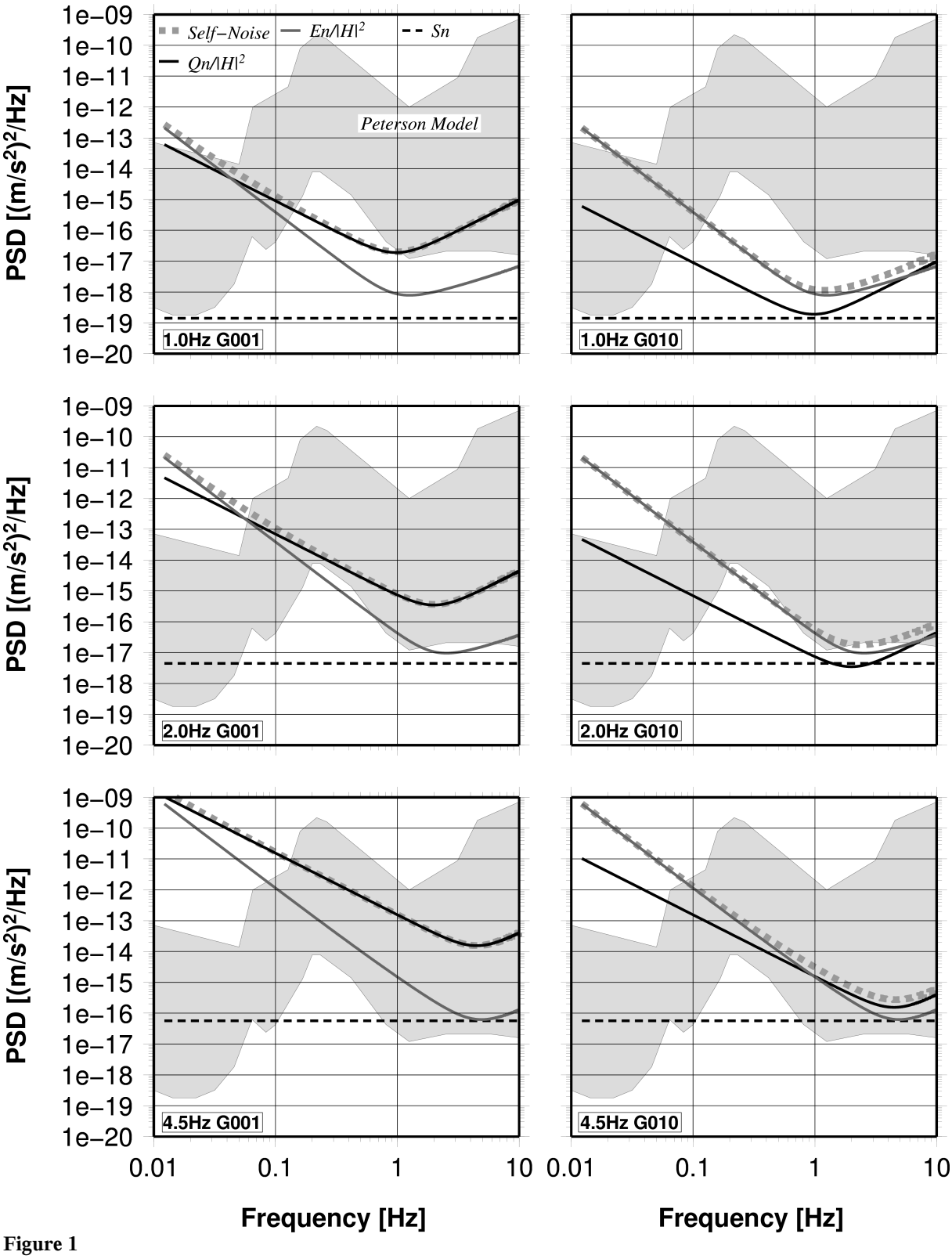
Self−Noise
En/|H|2
Sn
Qn/|H|2
Peterson Model
1.0Hz G001
1.0Hz G010
2.0Hz G001
2.0Hz G010
4.5Hz G001
4.5Hz G010
PSD [(m/s2)2/Hz]
1e−09
1e−10
1e−11
1e−12
1e−13
1e−14
1e−15
1e−16
1e−17
1e−18
1e−19
1e−20
0.01
0.1
1
10
Frequency [Hz]

Figure 1

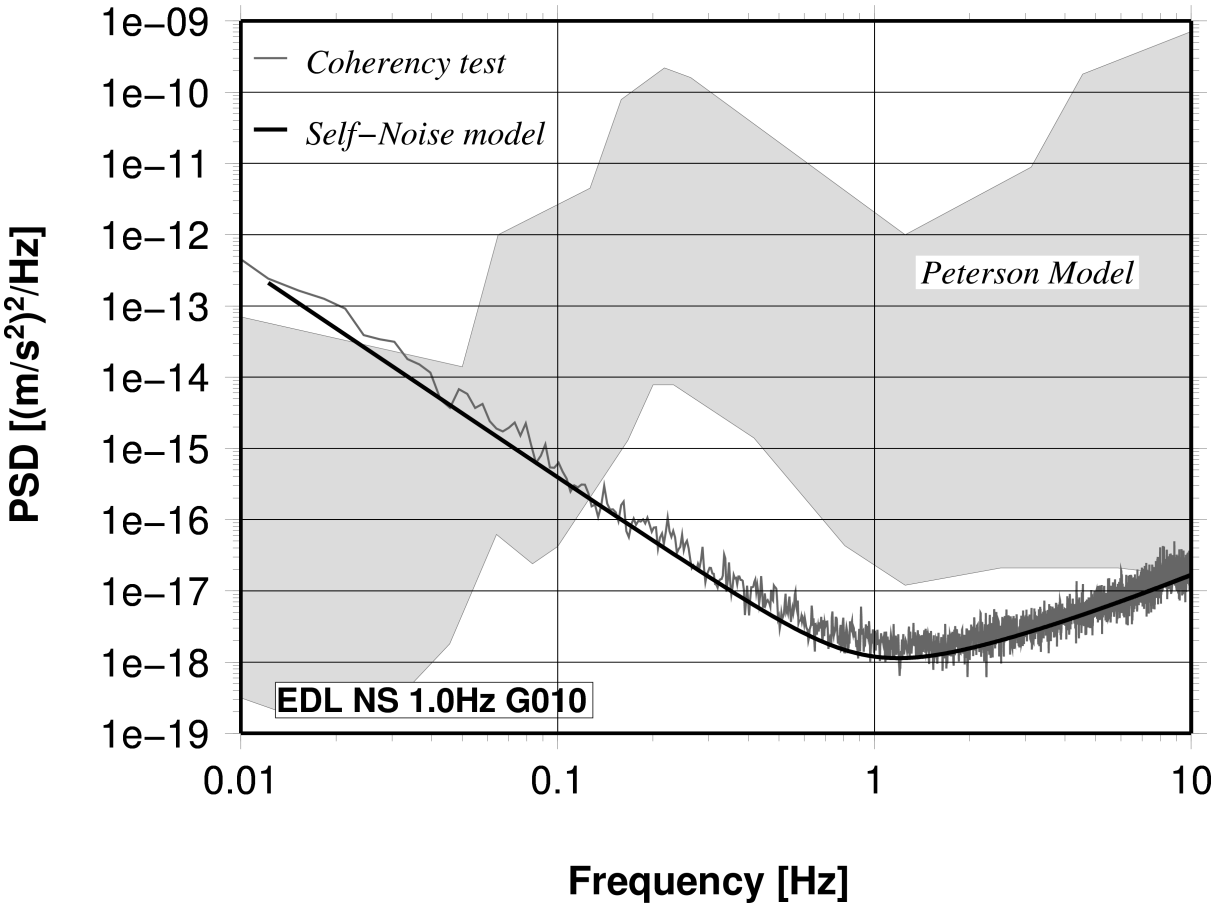
1e−09
1e−10
1e−11
1e−12
1e−13
1e−14
1e−15
1e−16
1e−17
1e−18
1e−19
PSD [(m/s²)²/Hz]
Coherency test
Self−Noise model
Peterson Model
EDL NS 1.0Hz G010
0.01
0.1
1
10
Frequency [Hz]

Figure 2

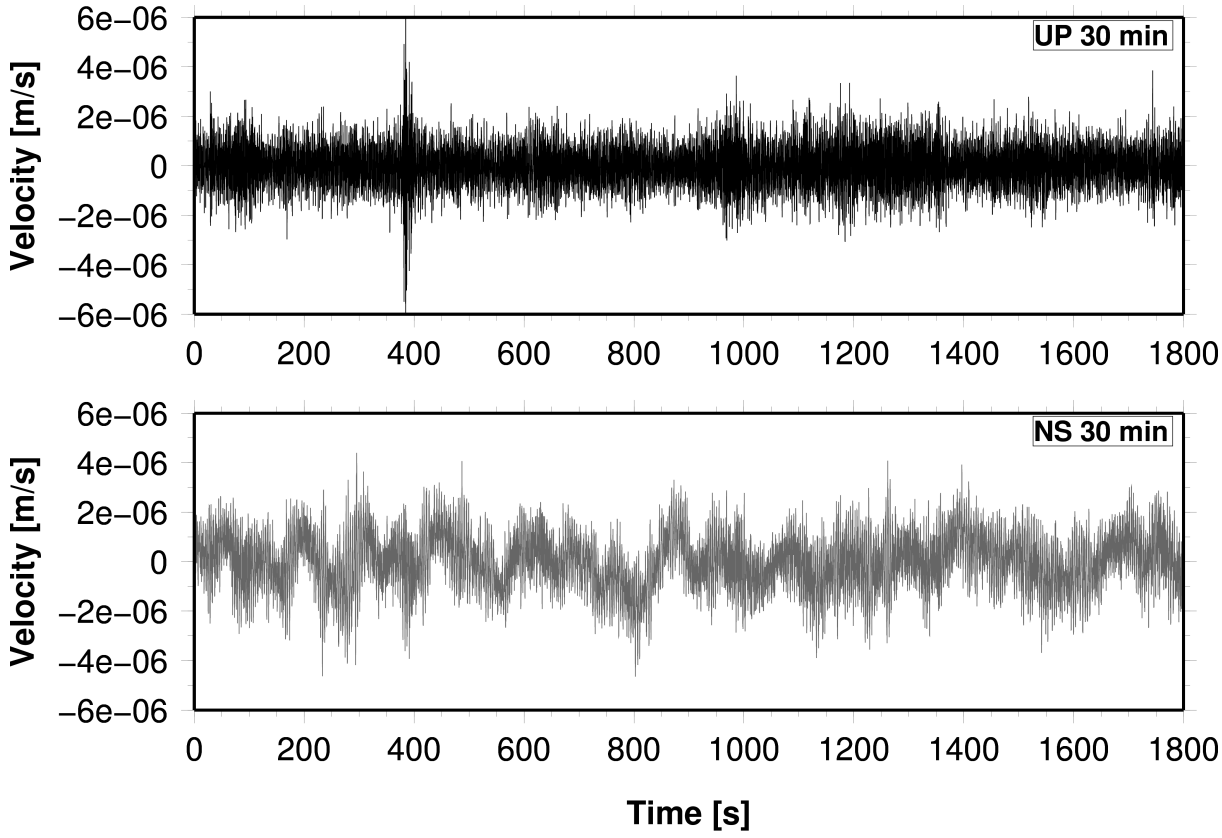
UP 30 min
NS 30 min
Velocity [m/s]
6e−06
4e−06
2e−06
0
−2e−06
−4e−06
−6e−06
0
200
400
600
800
1000
1200
1400
1600
1800
Time [s]

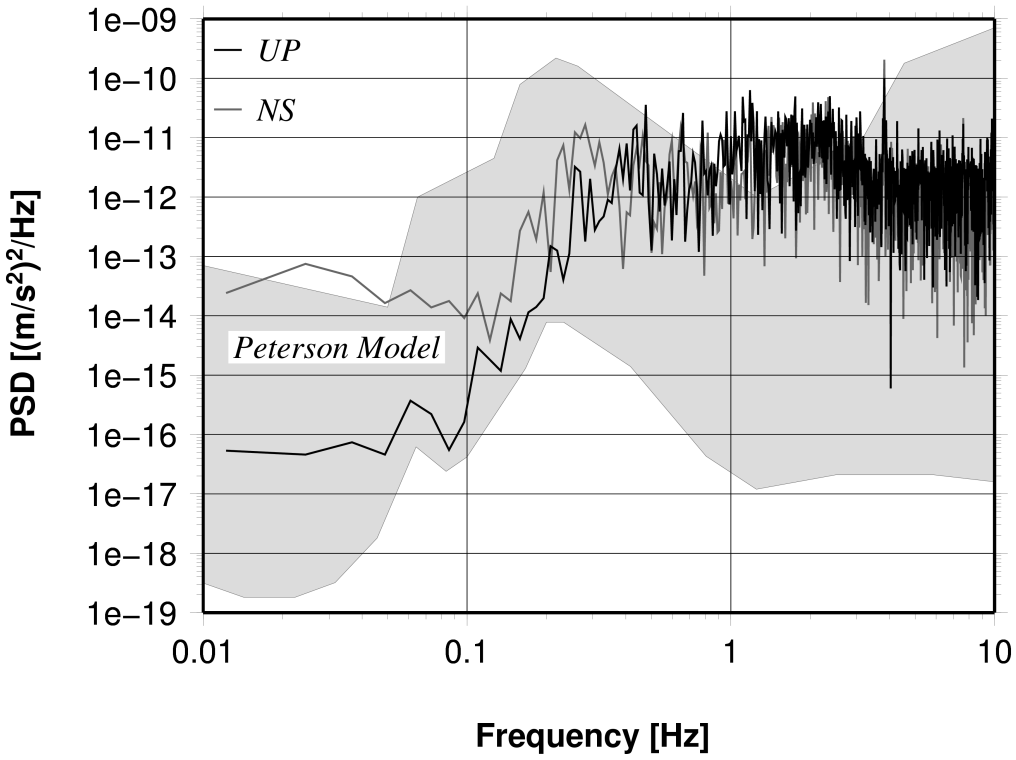
UP
NS
Peterson Model
PSD [(m/s²)²/Hz]
1e−09
1e−10
1e−11
1e−12
1e−13
1e−14
1e−15
1e−16
1e−17
1e−18
1e−19
0.01
0.1
1
10
Frequency [Hz]

Figure 3

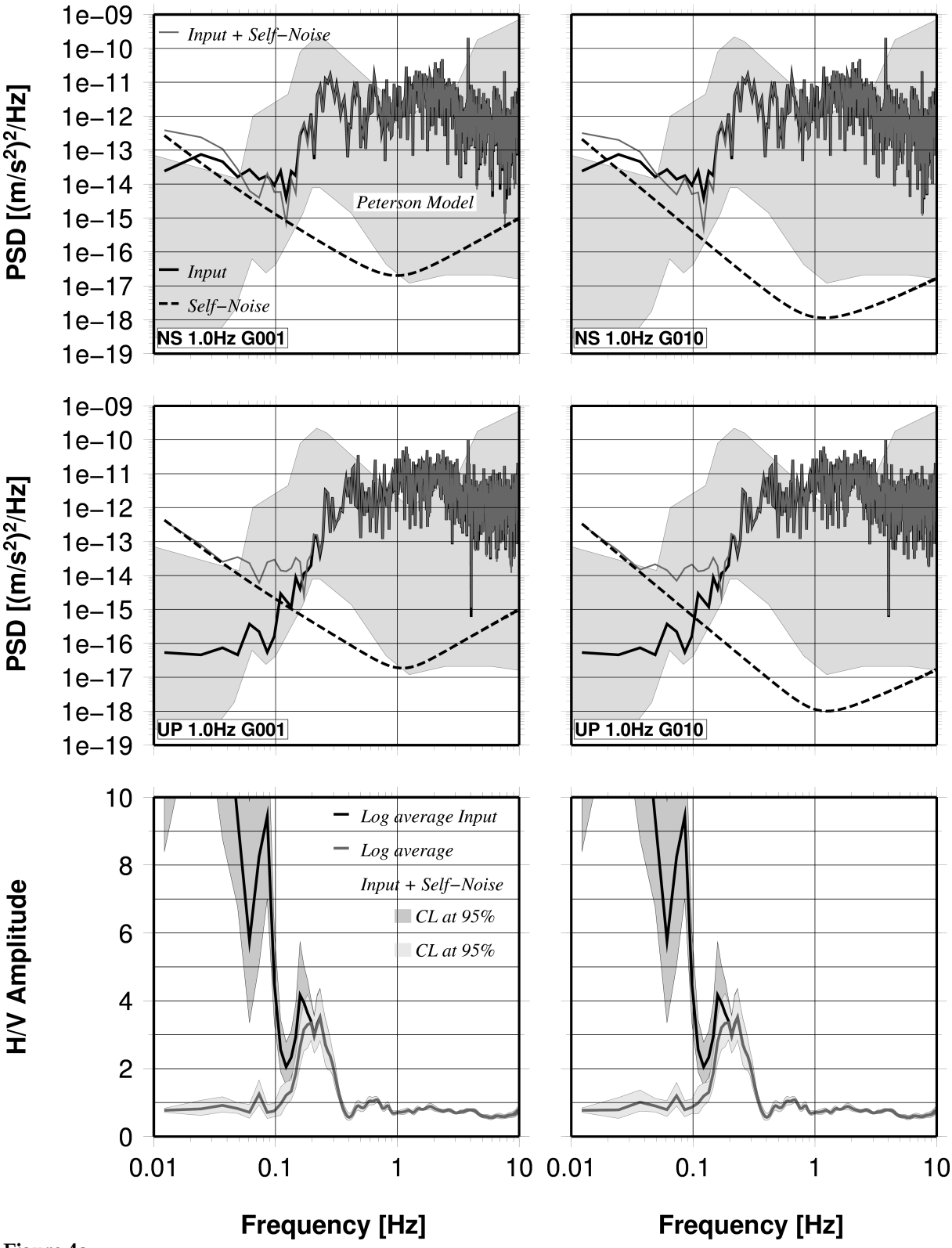
PSD [(m/s²)²/Hz]
1e−09
1e−10
1e−11
1e−12
1e−13
1e−14
1e−15
1e−16
1e−17
1e−18
1e−19
Input + Self−Noise
Peterson Model
Input
Self−Noise
NS 1.0Hz G001
NS 1.0Hz G010
UP 1.0Hz G001
UP 1.0Hz G010
H/V Amplitude
10
8
6
4
2
0
Log average Input
Log average
Input + Self−Noise
CL at 95%
CL at 95%
0.01
0.1
1
10
Frequency [Hz]

Figure 4a

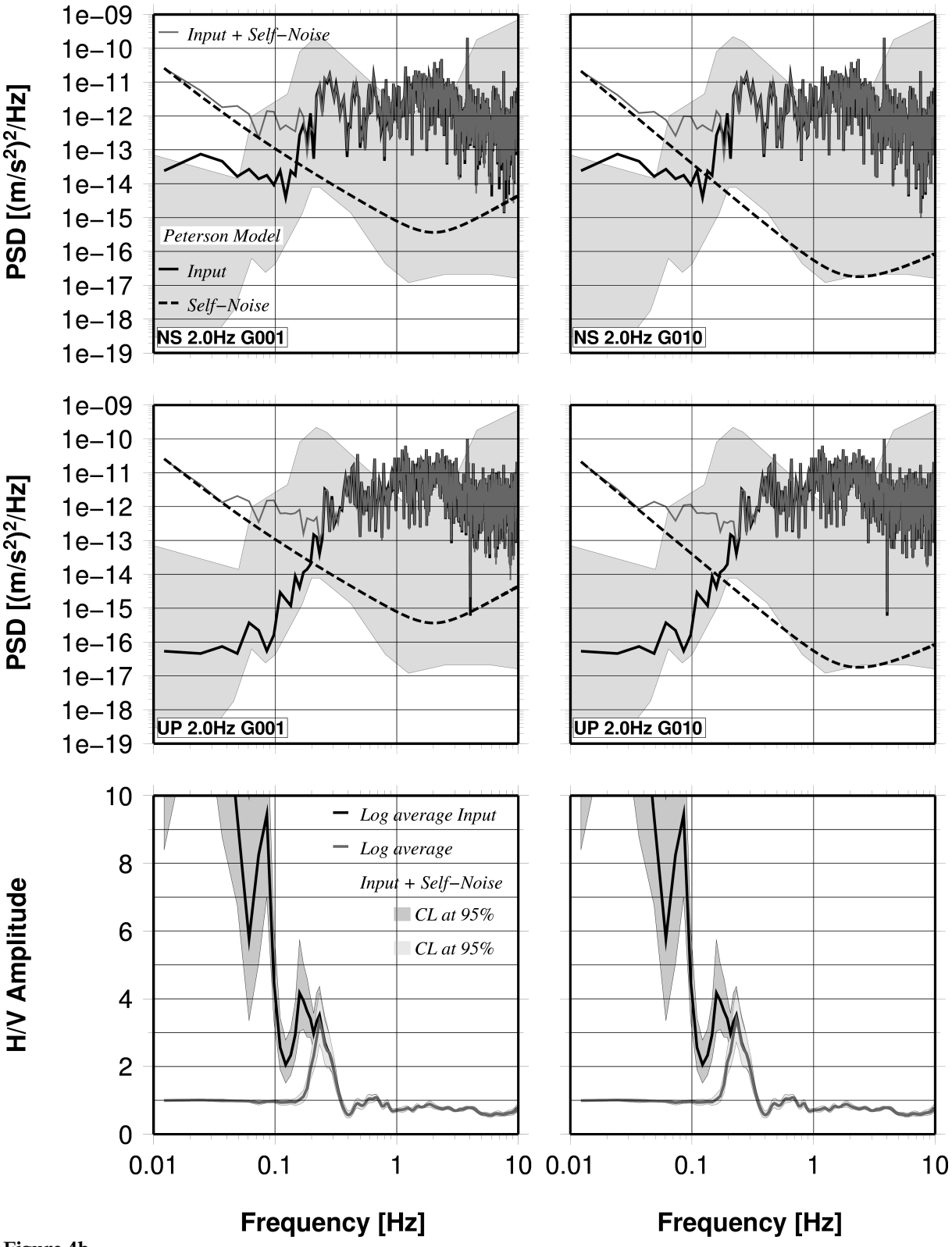
PSD [(m/s²)²/Hz]
1e−09
1e−10
1e−11
1e−12
1e−13
1e−14
1e−15
1e−16
1e−17
1e−18
1e−19
Input + Self−Noise
Peterson Model
Input
Self−Noise
NS 2.0Hz G001
NS 2.0Hz G010
UP 2.0Hz G001
UP 2.0Hz G010
H/V Amplitude
10
8
6
4
2
0
Log average Input
Log average
Input + Self−Noise
CL at 95%
CL at 95%
0.01
0.1
1
10
Frequency [Hz]

Figure 4b

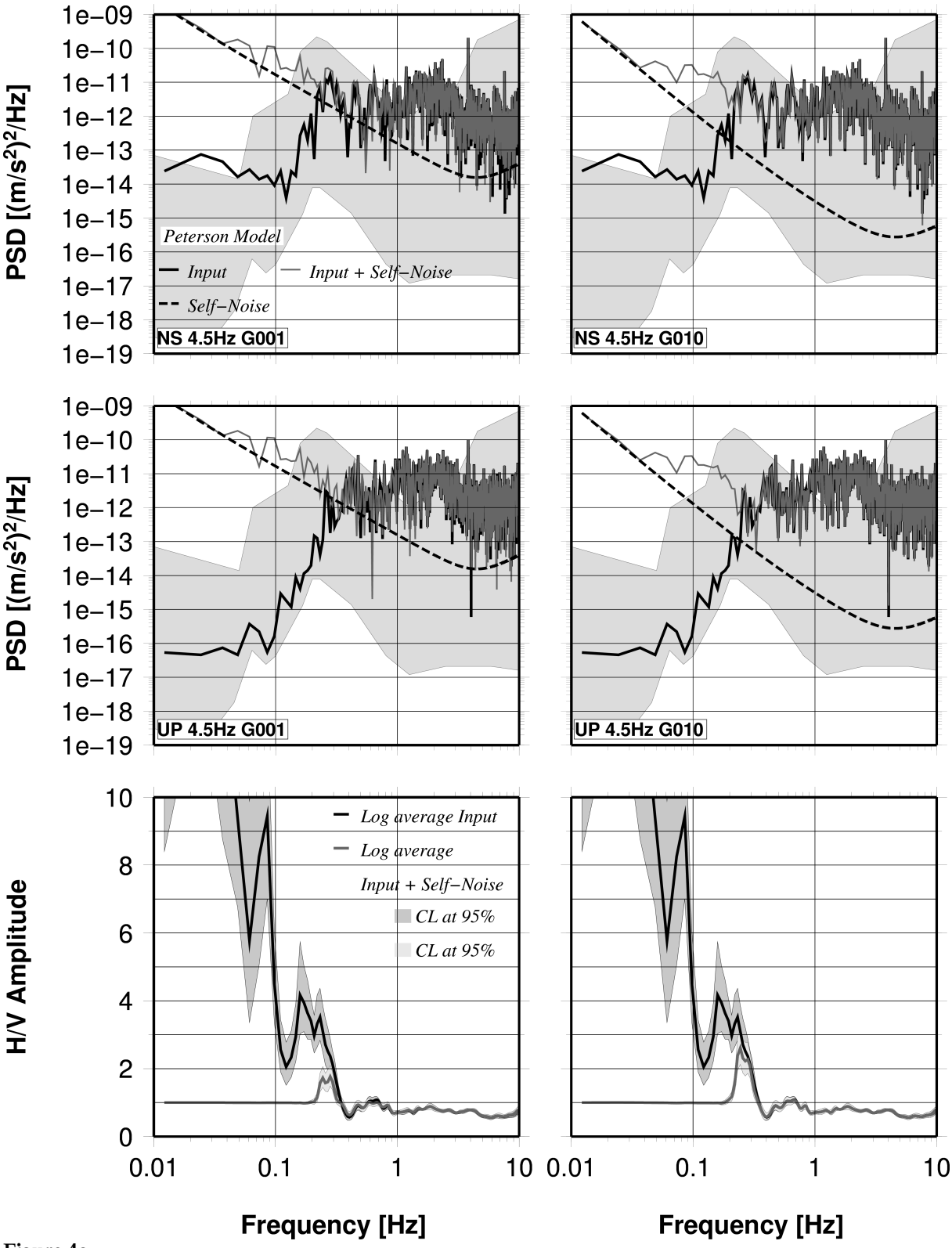
PSD [(m/s²)²/Hz]
1e−09
1e−10
1e−11
1e−12
1e−13
1e−14
1e−15
1e−16
1e−17
1e−18
1e−19
Peterson Model
Input
Input + Self−Noise
Self−Noise
NS 4.5Hz G001
NS 4.5Hz G010
UP 4.5Hz G001
UP 4.5Hz G010
H/V Amplitude
10
8
6
4
2
0
Log average Input
Log average
Input + Self−Noise
CL at 95%
CL at 95%
0.01
0.1
1
10
Frequency [Hz]

Figure 4c

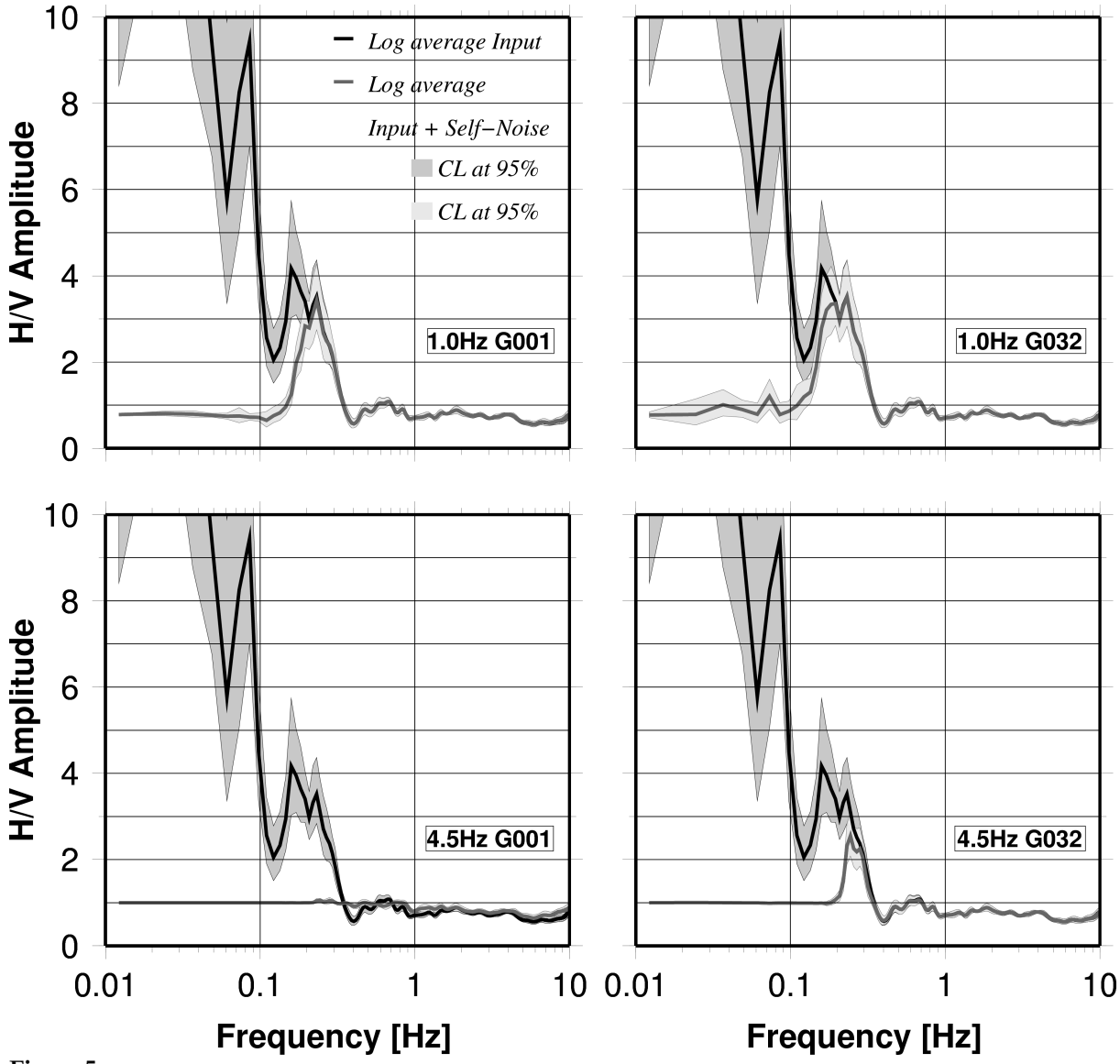
Log average Input
Log average
Input + Self−Noise
CL at 95%
CL at 95%
1.0Hz G001
1.0Hz G032
4.5Hz G001
4.5Hz G032
H/V Amplitude
H/V Amplitude
Frequency [Hz]
Frequency [Hz]
0
2
4
6
8
10
0.01
0.1
1
10

Figure 5